Electrochemical and Solid-State Letters, **8** (10) C148-C150 (2005)
1099-0062/2005/8(10)/C148/3/$7.00 © The Electrochemical Society, Inc.

Galvanic Deposition of Nanostructured Noble-Metal Films on Silicon

Yan-Yan Song,[a] Zhi-Da Gao,[b] John J. Kelly,[c,*] and Xing-Hua Xia[a,z]

[a]*Key Laboratory of Analytical Chemistry for Life Science, Department of Chemistry, Nanjing University, Nanjing 210093, China*
[b]*Department of Physics, National Laboratory of Solid State Microstructures, Nanjing University, Nanjing 210093, China*
[c]*Debye Institute, Utrecht University, 3584 CC Utrecht, The Netherlands*

Large-area nanostructured noble-metal films (Ag, Pt, and Au) can be deposited with high yields and various morphologies on silicon formed between the semiconductor and the noble metal by means of a galvanic cell. It is shown that the morphology of Ag, which is different from that of Pt and Au, can be influenced markedly by the deposition conditions. Distinctive surface-enhanced Raman-scattering features are observed on these Ag films.
 [DOI: 10.1149/1.2033616]

Manuscript submitted May 18, 2005; revised manuscript received June 22, 2005. Available electronically August 12, 2005.

Following the synthesis of carbon nanotubes,[1] one-dimensional and two-dimensional nanostructured materials have aroused increasing interest due to their exceptional properties and potential applications.[2-4] Compared to micrometer-diameter whiskers, nanowires are expected to have remarkable chemical and physical properties (e.g., optical, electrical, and magnetic) that are tunable by varying their length and diameter. Recent progress in materials science shows that metallic nanostructures also exhibit unusual optical, thermal, chemical, and physical properties due to a combination of a large ratio of surface-to-bulk atoms and to the nanometer-scale mean-free path of an electron in a metal ($\sim$10 to 100 nm for many metals at room temperature).[5-8] Nanostructured silver is one of the most widely investigated systems. Until now, different physical and chemical approaches have been explored for synthesizing the silver nanostructures. For example, silver nanostructures can be prepared by ultrasonic irradiation,[9,10] illumination,[11,12] by irradiating an aqueous silver salt solution with ultraviolet light in the presence of poly(vinyl alcohol),[13] by a soft self-seeding polyol process,[14] or by an ion-exchange technique.[15] Here we report another simple but fast method to synthesize large-area nanostructured noble-metal films with high yields and various morphologies.

We use an exchange reaction driven by a galvanic cell which is formed between silicon and the deposited metal in a solution containing the noble-metal ions. We compare the deposition of Au, Pt, and Ag. The morphology of the Ag layer is especially interesting, as it can be influenced markedly by varying the experimental conditions (Ag^+ ion concentration, temperature, use of surfactants, illumination and ultrasonic vibration). Features such as dendrites, spheres, "feathers," rods, and wires can be obtained. In addition, a distinctive surface-enhanced Raman scattering is observed with these nanostructured Ag films.

For more details on galvanic cells formed between silicon and metals we refer to our previous work,[16,17] in which the galvanic cell approach was used to realize various functions in silicon micromachining, e.g., porous silicon formation and selective passivation for etch-stop mechanisms.[17]

Experimental

The p-type single-crystal silicon (100) wafers were boron-doped with a resistivity in the range 1–15 Ω cm. Before each experiment, the silicon pieces were degreased by sonication in acetone and ethanol, and then rinsed with Millipore water (18 MΩ, Purelab Classic Corp., USA). All chemicals were of p.a. grade (Merck), and used as received. All solutions were prepared from Millipore water.

Electrochemical experiments were performed with a CHI 650 Electrochemical Workstation (CH Instrument, USA). A conventional three-electrode electrochemical cell was used with a Pt counter electrode and a saturated calomel electrode (SCE) as reference. The working electrode was a silicon wafer or a gold sheet (1 $\times$ 1 cm). Before each measurement, the silicon was dipped in a solution of 1 M HF + 2 M NH_4F for 1 min and washed with Millipore water to remove native oxide. The silicon working electrode was mounted in a Kel-F holder with an O-ring. Electrical contact to a brass disk on the back side of the sample was made using Ga/In eutectic. All potentials are referred to SCE. Ultrasound irradiation was carried out in a high-intensity ultrasound irradiation instrument (Kunshan Co., China, KQ-100 E, 40 kHz, 100 W) under constant temperature.

The morphology of the resulting structures was examined with an XL30 environment scanning electron microscope (ESEM, Philips). Surface-enhanced Raman spectra (SERS) were obtained with a HR-800 confocal microprobe Raman system (Jobin-Yvon, France). The exciting light was the 488 nm line from an internal Ar^+ ion laser with a power of 1 mW at the sample surface.

Results and Discussion

Galvanic cell formation.— When silicon is exposed to noble metal ions (M^{n+}) in aqueous HF solution an exchange reaction takes place. Because the redox potential of the M^{n+}/M couple is positive, the acceptor levels (M^{n+}) correspond to the valence band of the semiconductor; the metal ions are reduced by electron transfer from the valence band of the solid, i.e., holes are "injected" into the band

$$M^{n+} \rightarrow M + n h^+ \quad [1]$$

The holes are used for the oxidation of silicon. In HF solution each silicon atom can react with two holes and dissolve, producing one hydrogen gas molecule (Reaction 2).[16,17] Silicon goes to solution as a hexafluoride complex (Reaction 2)

$$Si + 2H^+ + 2h^+ \rightarrow Si^{4+} + H_2 \quad [2]$$

$$Si^{4+} + 6HF \rightarrow SiF_6^{2-} + 6H^+ \quad [3]$$

Once some metal has been deposited, further deposition can occur either on the bare surface or on existing metal. The latter is more likely, as deposition on bare surface requires the formation of fresh metal nuclei; this is generally less favorable.

When metal deposits preferentially on metal areas we have, in effect, a galvanic cell with silicon and the metal acting as local anode and cathode, respectively (Fig. 1). The operation of the cell can be understood on the basis of the potential dependence of the two partial reactions (1 and 2). Curve a of Fig. 1 gives the anodic oxidation of p-type Si in metal-free HF solution. At low current density (below the peak) porous silicon is formed. At potentials beyond the peak the semiconductor is polished. In contrast to Reaction 2, this is a four-hole reaction involving formation and dissolu-

* Electrochemical Society Active Member.
z E-mail: xhxia@nju.edu.cn

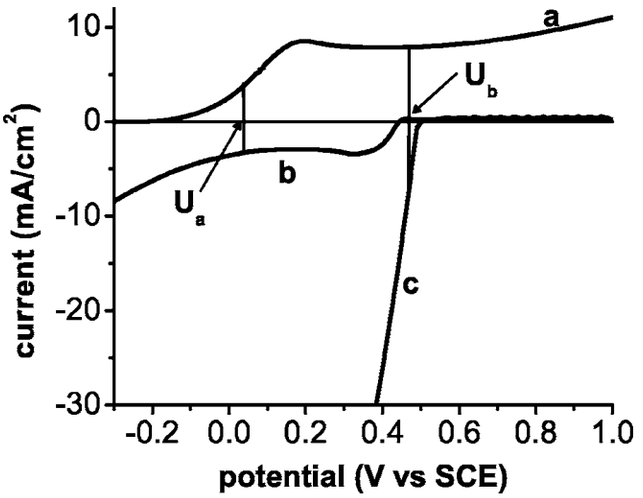

Figure 1. Electrochemical results demonstrating galvanic cell formation. Curve a shows the current-potential curve for a p-Si(100) electrode in a 5 M HF solution in the dark. Cathodic current-potential curves are shown for 20 mM (curve b) and 200 mM (curve c) $AgNO_3$ solutions measured at an Au electrode. The mixed-potential of the galvanic cells in 20 mM (U_a) and 200 mM (U_b) $AgNO_3$ solutions are also given. The scan rate was 5 mV/s.

tion of oxide.[16,17] Curve b of Fig. 1 shows the reduction of Ag^+ ions to Ag at a gold electrode in an aqueous HF solution. The potential of the Ag^+/Ag couple (0.557 V vs SCE) is clearly much more positive than the onset potential for anodic oxidation of silicon. Two Ag^+ ion concentrations are considered in Fig. 1. At the lower concentration (curve c) a well-defined diffusion plateau is observed, while at higher concentration (curve c), the reduction current is much higher (the limiting current is not shown in the figure). When p-Si and Ag-on-Au are short-circuited, the open-circuit potential, at which the Si oxidation and Ag^+ reduction rates are equal, is in the onset range of the anodic current-potential curve for the lower concentration, i.e., deposition is accompanied by the formation of porous silicon. When the reduction current is much higher (curve c of Fig. 1) a more positive open-circuit potential is observed and deposition occurs under polishing conditions.

From Fig. 1 it is clear that open-circuit metallization of silicon should depend on a variety of factors: the kinetics of nucleation and growth of the metal on silicon and subsequently on the metal, the kinetics of silicon oxidation, and the hydrodynamics of the system (both partial reactions in Fig. 1 can be mass-transport controlled). Depending on the metal and the experimental conditions one might expect different metal morphologies.

Metal deposition.— In Fig. 2 we show results for three metals (Pt, Au, and Ag) deposited under the same conditions. In each case, a 20 mM metal ion, 5 M HF solution was used at 45°C. Deposition was carried out in the dark for 60 min. In H_2PtCl_6 and $HAuCl_4$ solution three-dimensional particulate layers were formed with particle dimensions of about 450 nm (see Fig. 2a and b). A layer of three-dimensional Pt and Au nanoparticles with spherical structures and triangle structures formed respectively. In both cases, an fcc structure was confirmed by X-ray diffraction measurements, which revealed a predominant (111) orientation in the spectra. On the other hand silver grown from $AgNO_3$ solution was dendritic, giving branched nanostructures (Fig. 2c). Such strongly oriented growth is often encountered in silver electrodeposition.[9,10,18,19] The main branches and the side branches had dimensions of about 450 and 200 nm, respectively. Silver deposited at short times (less than 2 min) adheres strongly to the substrate and can only be removed by scratching. For a deposition time of less than about 10 min the silver nanostructures grow mainly perpendicular to the surface. At longer

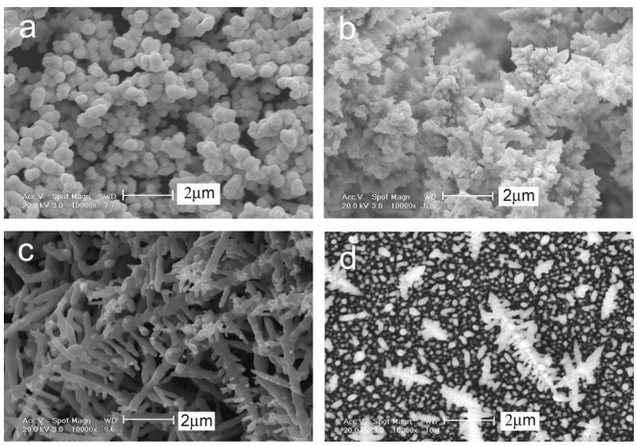

Figure 2. SEM images of (a) Pt, (b) Au, and (c) Ag deposits formed galvanically on p-Si(100) wafers in the dark from a 5 M HF solution containing 20 mM $HAuCl_4$, 20 mM H_2PtCl_6, and 20 mM $AgNO_3$ respectively. (d) The transition to a Ag dendritic morphology (2 mM $AgNO_3$, 1 h). The solution temperature was 45°C.

deposition times the deposit begins to branch, giving three-dimensional structures; the onset of dendritic growth is clear in Fig. 2d).

Figure 3 demonstrates some of the distinctive silver morphologies that can be obtained. In all cases, metal was deposited from a 0.02 M $AgNO_3$ solution at 25°C. Figure 3a is a reference dendritic sample obtained with a deposition time of 60 min in an unstirred solution. Figure 3b shows the effect of ultrasonic vibration, also for a deposition time of 60 min. In this case, the ends of the branches convert to balls with diameters of about 400 nm. The combination

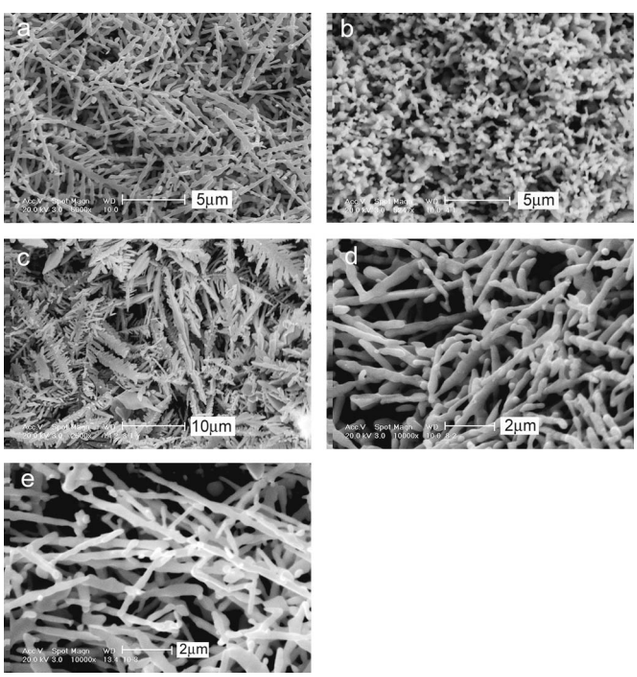

Figure 3. SEM images of galvanically deposited Ag nanostructures on p-Si (100) wafers from a 20 mM $AgNO_3$, 5 M HF solution in the dark at 25°C. (a) Deposition for 1 h. (b) Deposition for 1 h with ultrasonic vibration. (c) Deposition for 1 h with ultrasonic vibration with 1% PVP in solution. (d) Deposition for 30 min from a solution which also contained PEG. (e) Deposition for 60 min from a solution which also contained PEG.

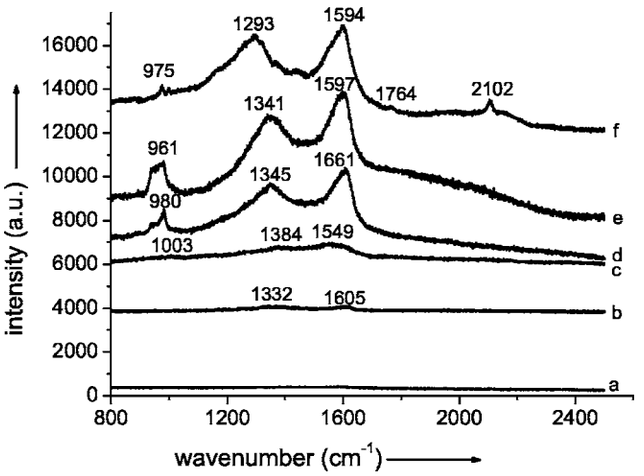

Figure 4. Surface Raman spectra of pyridine adsorbed on (a) flat Ag and different Ag nanostructures corresponding to (b) dendrites, (c) rods, (d) balls, (e) wires, and (f) feathers. The solution contained 0.01 M pyridine and 0.1 M KCl.

of a surface-active agent, polyvinylpyrrolidone (PVP), and ultrasonic vibration gives a "feather-like" morphology (Fig. 3c). Deposition for 30 min from a solution with the surfactant PEG-2000 gives rods (Fig. 3d) which grow to wires at longer deposition times (Fig. 3e).

Surface-enhanced Raman.— Both experiments and theoretical calculations show that the optical properties of nanomaterials depend on the nature of the metal and its surface morphology.[20] Theoretical work has predicted that the surface-enhanced Raman scattering (SERS) intensity could be increased by using nanocrystals with enhanced aspect ratio.[21-25] Our preliminary Raman results with, as model system, pyridine on Ag prepared by the present methods confirm this prediction. The Raman spectrum for a flat Ag surface is almost featureless (Fig. 4, curve a). With Ag nanostructures deposited on silicon wafers, enhanced characteristic features are obvious (Fig. 4, curves b-f). The enhancement factor of the bands depends considerably on the Ag morphology. For dendrites (morphology of Fig. 2c) the enhancement factor is quite low and only a few pyridine features are observable (Fig. 4, curve b). In contrast, all the characteristic spectral features for adsorbed pyridine and the largest surface-enhancement factor could be observed (Fig. 4, curve f) on a featherlike Ag nanostructured surface (morphology of Fig. 3c).

The three major bands in curves a-f in Fig. 4 located at about 1000, 1300, and 1600 cm^{-1} are attributed to the ring breathing (υ_1), C–H in-plane deformation (υ_{6a}), and ring stretching (υ_{8a}) vibrations, respectively. And the bands at ca. 1700 and 2100 cm^{-1} can be attributed to the stretching mode of C=N. Obviously, such shape-dependent Raman spectra with different surface-enhancement factors must be due to the differences in the morphology of the nanostructure. In our case, the featherlike nanostructures consist of numerous ordered, oriented, and compacted nanowires. Such a morphology provides a suitable microenvironment for the adsorption of the pyridine molecule via the electron lone pair of the nitrogen.[26] Consequently, numerous microscopic ordered arrays of pyridine molecules can be adsorbed on the featherlike nanostructures of silver. Such a nanostructure is suitable for the Raman enhancement and could find application in Raman analysis.

References

1. S. Iijima, *Nature (London)*, **354**, 56 (1991).
2. P. M. Ajayan and S. Iijima, *Nature (London)*, **361**, 333 (1993).
3. C. Z. Li and N. J. Tao, *Appl. Phys. Lett.*, **72**, 894 (1998).
4. A. M. Moreal and A. M. Lieber, *Science*, **279**, 894 (1998).
5. M. A. El-Sayed, *Acc. Chem. Res.*, **34**, 257 (2001).
6. C. J. Murphy, *Science*, **298**, 2139 (2002).
7. M. Valden, X. Lai, and D. W. Goodman, *Science*, **281**, 1647 (1998).
8. K. K. Caswell, C. M. Bender, and C. J. Murphy, *Nano Lett.*, **3**, 667 (2003).
9. V. G. Pol, D. N. Srivastava, O. Palchik, V. Palchik, M. A. Slifkin, A. M. Weiss, and A. Gedanken, *Langmuir*, **18**, 3352 (2002).
10. J. J. Zhu, X. H. Liao, X. N. Zhao, and H. Y. Chen, *Mater. Lett.*, **49**, 91 (2001).
11. W. Wang and A. Asher, *J. Am. Chem. Soc.*, **123**, 12528 (2001).
12. A. Callegari, D. Tonti, and M. Chergui, *Nano Lett.*, **3**, 1565 (2003).
13. Y. Zhou, S. H. Yu, C. Y. Wang, X. G. Li, Y. R. Zhu, and Z. Y. Chen, *Adv. Mater. (Weinheim, Ger.)*, **11**, 850 (1999).
14. Y. G. Sun and Y. N. Xia, *Adv. Mater. (Weinheim, Ger.)*, **14**, 833 (2002).
15. L. Dloczik and R. Könenkamp, *Nano Lett.*, **3**, 651 (2003).
16. X. H. Xia, C. M. A. Ashruf, P. J. French, and J. J. Kelly, *Chem. Mater.*, **12**, 1671 (2002).
17. J. J. Kelly, X. H. Xia, C. M. A. Ashruf, and P. J. French, *IEEE Sensor J.*, **1**, 127 (2001).
18. K. Q. Peng, Y. J. Yan, S. P. Gao, and J. Zhu, *Adv. Mater. (Weinheim, Ger.)*, **14**, 1164 (2002).
19. K. Q. Peng, Y. J. Yan, S. P. Gao, and J. Zhu, *Adv. Funct. Mater.*, **13**, 127 (2003).
20. J. L. Yao, G. P. Pan, K. H. Xue, D. Y. Wu, B. Ren, D. M. Sun, J. Tang, X. Xu, and Z. Q. Tian, *Pure Appl. Chem.*, **72**, 221 (2000).
21. R. K. Chang, *Ber. Bunsenges. Phys. Chem.*, **91**, 296 (1987).
22. M. Moskovits, *Rev. Mod. Phys.*, **57**, 783 (1985).
23. M. Kerker, *Acc. Chem. Res.*, **17**, 271 (1984).
24. G. C. Schatz, *Acc. Chem. Res.*, **17**, 370 (1984).
25. C. Zuo and P. W. Jagodzinski, *J. Phys. Chem. B*, **109**, 1788 (2005).
26. M. Green and F. M. Liu, *J. Phys. Chem. B*, **107**, 13015 (2003).